https://doi.org/10.5194/bg-2020-330
Preprint. Discussion started: 8 October 2020

Biogeosciences Discussions Open Access EGU

Intersecting Methane Production and Oxidation Zones in Freshwater Sediments

Xueping Chen[a], Juan Yu[a], Lihua Liu[b,*], Jing Sun[a], Fayan Bai[a], Ming Yang[a], Zheng Chen[c], Chiquan He[a], Xiaoyan Liu[a], Shuang Bai[a], Fushun Wang[a,*]

[a]School of Environmental and Chemical Engineering, Shanghai University, 99 Shangda Road, Shanghai 200444, China

[b]Guangzhou Institute of Energy Conversion, Chinese Academy of Sciences, Guangzhou 510640, China

[c]Department of Health and Environmental Sciences, Xi'an Jiaotong-Liverpool University, Suzhou, Jiangsu 215123, China

Xueping Chen: xpchen@shu.edu.cn
Juan Yu: yjenviro@shu.edu.cn
*Lihua Liu: liulh@ms.giec.ac.cn
Jing Sun: mlyoung@shu.edu.cn
Fayan Bai: bfy0720@shu.edu.cn
Ming Yang: mingyang@shu.edu.cn
Zheng Chen: Zheng.Chen@xjtlu.edu.cn
Chiquan He: cqhe@shu.edu.cn
Xiaoyan Liu: lxy999@shu.edu.cn
Shuang Bai: hoarfrost@shu.edu.cn
*Fushun Wang: fswang@shu.edu.cn

*Corresponding author

Lihua Liu, Tel: +86 20 37223742. Fax: +86 20 37223742.

Fushun Wang, E-mail: Tel: +8602166137502. Fax: +8602166137502

https://doi.org/10.5194/bg-2020-330
Preprint. Discussion started: 8 October 2020


Biogeosciences Discussions

Abstract

Methane is produced and emitted when organic carbon accumulates in the sediments of reservoirs. Before being released into the water body, methane can be oxidised microbially by multiple electron accepters in the sediment, and which were traditionally considered to be spatially separated from methanogens. This study provides geochemical and microbiological evidence to firstly demonstrate that methane production and oxidisation zones intersected each other in the sediment of a freshwater reservoir. Methanogens were distributed along the sediment depth profile. Hydrogenotrophic *Methanomicrobiales* were found to be responsible for methane production in the upper layer (< 20 cm), Hydrogenotrophic might be an active methanogenic pathway in the upper layers. Whereas *Methanobacteriales* and aceticlastic *Methanosarcinales* were responsible for methane production in the deeper layer, and aceticlastic pathway in the deeper layer. Meanwhile, the findings showed that methane was oxidised along the sediment profile. Sulfate and iron-dependent methane oxidisation dominated the surface layer and nitrite-dependent methane oxidisation prevailed in the middle layer (14–24 cm). However, the range of the sulfate zone (< 7 cm) extended deeper than the iron zone (< 5 cm). The relative abundance of *Desulfobulbus* and iron-oxidising bacteria (*Ferritrophicum* and *Crenothrix*) confirmed the concurrence of the sulfate and iron anaerobic-oxidation of methane (AOM) zones in the surface layer. Both of the AOM potential activity and nitrite peak indicated the active nitrite-AOM below sulfate-AOM zone. In addition to the complex crossing pattern of methane production and consumption, this work revealed a high potential of

https://doi.org/10.5194/bg-2020-330
Preprint. Discussion started: 8 October 2020


Biogeosciences Discussions Open Access EGU

48 AOMs which would prevent *in situ* methane emissions from freshwater environments.
49 A further investigation for the mechanism of the niche partitioning of methanogens and
50 methane oxidizers in various types of reservoirs and the controlling factor on the
51 distribution pattern is necessary.

52 **Keywords:** methanogens; methane oxidation; methane emission; microbial activity;
53 archaea

https://doi.org/10.5194/bg-2020-330
Preprint. Discussion started: 8 October 2020


Biogeosciences Discussions

1. Introduction

There is an increasing interest and concern regarding greenhouse gas emissions from natural lakes and artificial reservoirs. Collectively, these represent one of the largest natural sources of methane, a greenhouse gas, with an estimated global emission of 12–70 Tg y^{-1} (Barros et al. 2011; Deemer et al. 2016), which accounts for 6–16% of the annual natural methane emissions (Goldman et al. 2016). The sediments of lakes and reservoirs receive much more excessive labile organic matter in comparison to ocean sediments. Although the quantitative estimates of the terminal methane emission flux from lakes/reservoirs are well known through direct measurements and large-scale modelling (Maeck et al. 2013), the transformation and mechanism of these processes in sediments at a small-scale receive inadequate attention.

Microbial processes control methane production and consumption in addition to methane diffusion and advection in sediments. Methane in the sediments of anoxic lakes/reservoirs is produced via the microbial decomposition of organic matter. Although lake/reservoir sediments are commonly viewed as 'hot spots' of methane production (Bastviken et al. 2004), it has been estimated that 50–95% (median of 90%) of the methane produced in freshwater lakes is oxidised before it reaches the atmosphere (Bastviken et al. 2008). Biological methane-oxidation is carried out by methanotrophs through aerobic and/or anaerobic processes. The oxic layer of sediments, or that in the overlying water, is believed to be the main site for methane-oxidisation in lakes (Bastviken et al. 2008). Recent research has implied that the anaerobic oxidation of methane (AOM) can occur in non-marine sediments via

https://doi.org/10.5194/bg-2020-330
Preprint. Discussion started: 8 October 2020

denitrification (Ettwig et al. 2010), sulfate reduction (Beal, House, and Orphan 2009; Nordi, Thamdrup, and Schubert 2013), and iron reduction in either a direct coupling or through the re-oxidation of sulfide (He et al. 2018).

Based on the classical redox reactions sequence, the microbially mediated reactions are listed as denitrification, iron reduction, sulfate reduction and methanogenic in a thermodynamic order. However, some reactions may overlap or reverse in the natural environment, and the boundaries of the reaction zone may cross. Generally, biogenic methane is produced in the anoxic layers of sediment and consumed during its upward migration in marine (Egger et al. 2015; Riedinger et al. 2014) and coastal sediments (He et al. 2019). However, because of the complex environment conditions and multiple redox ions in the sediments, various ecological niches of methane production and consumption have been found. Sivan et al. (Sivan et al. 2011) proposed that the metal-AOM occurred below the zone of methanogenesis where nitrate and sulfate were completely removed. On the contrary, Metal-AOM and sulfate-AOM occurred simultaneously in the surface sediments in Lake Ørn (Nordi and Thamdrup 2014). It is putative that metal-AOM was located slightly below the oxic/anoxic interface in iron-rich lake and stratified lake waters (Crowe et al. 2011). In addition, anthropogenic eutrophication (Egger et al. 2015) and rapid sediment deposition (Riedinger et al. 2014) could trigger the up-shift of sulphate-methane transition zone (SMTZ) in costal sediments. Given the complex redox environment in reservoir sediment, we hypothesise that methane production and oxidation may coexist in freshwater as well as in coastal sediments (Maltby et al. 2018; Sivan et al. 2011), and

https://doi.org/10.5194/bg-2020-330
Preprint. Discussion started: 8 October 2020

that the chemical gradient along a sediment profile may lead to a niche differentiation of the AOM depending on the type of electron acceptor.

To test this hypothesis, we investigated sediment cores collected from Hongfeng Reservoir. The reservoir is a lake-type reservoir that has a large amount of nutrients and pollutants in its sediments, which have accumulated since the reservoir was constructed in 1958. In particular, we studied (1) the spatial pattern of methane production and oxidation zones along the sediment cores; (2) the microbial drivers responsible for the specific pattern; (3) the role of electron acceptors, including iron, sulfate, and nitrite, in regulating methane oxidisation. To achieve these objectives, the geochemical characteristics and microbial communities were studied in the collected sediments.

2. Materials and Methods

2.1. Site description and sample collection

Hongfeng Reservoir is a eutrophic lake-type reservoir located in Qingzhen, Guizhou Province, China (106°19'–106°28' E, 26°26'–26°35' N, Fig. S1). The reservoir has a storage capacity of 6.01×10^8 m^3 and an average (maximum) water depth of 10.5 m (45 m). Surface water samples and one sediment core (diameter of 65 mm) were collected from the central area of the reservoir (106.4151 °E, 26.478533 °N) with a 10 m water depth in January 2017 (Fig. S1). Before the sediment core was collected, several parameters were measured *in-situ* using a water quality analyser (YSI Weiser Pro 2030, Ohio, USA). The measured parameters included temperature (10.5 ℃), pH (8.1), salinity (0.18 PSU), and dissolved oxygen (9.26 mg L^{-1}). The core was ~38 cm in length, and reached the soil layer corresponding to the period before the construction of the

https://doi.org/10.5194/bg-2020-330
Preprint. Discussion started: 8 October 2020

dam. The surface sediments (~1 cm) were dark brown (Fig. S1) and may have contained iron oxides, whereas the deeper sediments were black. The sediment core was cut *in-situ* into 1 cm (0–20 cm) or 2 cm (20–38 cm) sub-samples. Porewater was extracted simultaneously using a Rhizon sampler (Rhizosphere Research Products, The Netherlands) connected to vacuum sampling bottles, and was then stored at 4 ℃. Some of the solid samples were frozen at -20 ℃ for DNA extraction and sequencing, and some were kept at 4 ℃ for later incubation. Aliquots of sediments were dried in an oven at 105 ℃ for 12 h and then filtered through a 200-mesh strainer. Some aliquots were powdered manually in an agate mortar for subsequent geochemical analysis.

2.2. Geochemical analytical methods

2.2.1. Sediment sample analyses

A subsample was decalcified with 10% HCl before being washed twice with deionised water and dried at 50 ℃ for total organic carbon (TOC) determination using a CHN-O rapid elemental analyser (Heaeus, Germany).

2.2.2 Determination of components and isotopic compositions of porewater

The concentrations of anions (SO_4^{2-} and NO_2^-) in the porewater were determined using an ion chromatographer (IC; ICS-1100, Thermo, CA, USA) with a column of AG 19 (4 mm ×250 mm). The porewater concentrations of formic acid, acetic acid, and propionic acid were analysed using an IC equipped with a column of Ion Pac AS11-HC (4 mm × 250 mm). Dissolved iron was determined by inductively coupled plasma mass-spectrometry (ICP–MS; Thermo iCAP Q, CA, USA) after samples were first diluted with 1% HNO_3.

https://doi.org/10.5194/bg-2020-330
Preprint. Discussion started: 8 October 2020

The concentrations and stable carbon isotopic ($\delta^{13}C$) compositions of CH_4 and CO_2 from the porewater were determined by gas chromatography (GC; GC-C/TC III) isotope-ratio mass spectrometry (IRMS; Delta V Advantage IRMS) and trace ultra GC (Thermo Finnigan). The chromatographic column was a HP-PLOT Q (30 m × 0.32 mm × 20.00 μm; J & W), and the injection temperature was 120 ℃ at a speed of 1.5 mL min^{-1}. The temperature of the burner was 960 ℃, and that of the reducing furnace was 600 ℃. The precision of the $\delta^{13}C_{CH4}$ and $\delta^{13}C_{CO2}$ measurements was ± 0.2‰. The concentration and carbon isotopic compositions of dissolved inorganic carbon (DIC) were determined using GasBench-IRMS (Delta V Advantage, USA).

2.3. Laboratory incubation

To measure the methane production potential, fresh sediment (equivalent to a 5.0 g dry weight) was placed into a 125 mL serum bottle using a cap-cut syringe. The serum bottles with sediments were vacuumed and gas charged with N_2 for three cycles to ensure anaerobic conditions. The bottles were immediately sealed with thick butyl rubber stoppers and aluminium caps and incubated in a 25 ℃ incubator. In addition, acetate (3.0 mmol kg^{-1}) was added as a substrate for methanogens. For the AOM potential measurement, the sediment incubation experiment was conducted as above, and was supplemented with methane at an initial concentration of approximately 8.3 mL L^{-1} after N_2 replacement in the headspace before being sealed. The headspace gas (1 mL) was collected by a micro-syringe for daily methane measurements. To maintain the pressure, 1 mL of pure N_2 was injected into the bottle. The CH_4 concentration was determined by GC (GC-900, Shanghai Kechuang Chromatography Instrument Co.

https://doi.org/10.5194/bg-2020-330
Preprint. Discussion started: 8 October 2020

Shanghai, China) with a hydrogen flame ionisation detector (FID), and was calculated per kilogram of dry weight (gdw) of sediment (Wassmann et al. 1998). All of the incubation experiments for methane production/oxidation potential were conducted in triplicate.

2.4. Microbial community

The DNA of sediment samples was extracted using a FastDNA® Spin Kit for Soil according to the manufacturer's instructions. The quality and concentration of the extracted DNA was determined via spectroscopic analysis (NanoDrop Technologies).

2.4.1 Illumina sequencing and analysis

The microbial communities of the collected sediments were analysed by Illumina MiSeq sequencing. Microbial sequencing was performed using the MiSeq Illumina platform at Meiji Biotechnology Company (Shanghai, China) according to the methods of Caporaso et al. (Caporaso et al. 2012) . Briefly, the V3–V4 and V4 regions of 16S bacterial and archaeal ribosomal DNA (rDNA) were amplified, respectively. The custom degenerate primer pairs of barcode-338F (5'-ACTCCTACGGGAGGCAGC-3')/907R (5'-CCGTCAATTCMTTTRAGTTT-3') and barcode-524F10extF (5'-TGYCAGCCGCCGCGGTAA-3') (570 bp)/Arch958RmodR (5'-YCCGGCGTTGAVTCCAATT-3') (434 bp) were used to generate an amplicon to construct libraries for bacteria and archaea, respectively. After sequencing, the quality of the raw data was checked (FastQC v0.11.8)) and filtered (PRINSEQ), and the sequences of < 400 bp were removed from the resultant data. In total, 561 817 and 2 067 765 unique sequences were ultimately obtained for bacteria and archaea,

https://doi.org/10.5194/bg-2020-330
Preprint. Discussion started: 8 October 2020

186 respectively.

187 The sequence data were analysed using QIIME (version 1.17) (Deemer et al. 2016),
188 and the sequences with a similarity of > 97% were clustered using Usearch (version 7.0,
189 http://drive5.com/uparse/). This resulted in 6132 and 1885 operational taxonomic units
190 (OTUs) for bacteria and archaea, respectively. The taxonomic assignment was
191 performed using the Ribosomal Database Project (RDP) classifier (Goldman et al.
192 2016) and a training set extracted from the Silva108 database (Mendonça et al. 2012).
193 Based on the results of the OTU clustering and annotation analysis, further data analysis
194 was performed using the Mage's I-Sanger platform (http://www.i-sanger.com/), which
195 integrates various R language packages for microbial community analysis. All
196 sequences were submitted to the Sequence Read Archive under the BioProject
197 accession numbers SAMN09011655 to SAMN09011709.

198 ***2.4.2 Quantitative PCR***

199 Copy numbers of the functional genes (*mcr*A) were determined by real-time
200 polymerase chain reaction (PCR) using an iCycleriQ 5 thermocycler (Bio-Rad, CA,
201 USA). The PCR primers were MLF
202 (5'GGTGGTGTMGGATTCACACARTAYGCWACAGC3') and MLR
203 (TTCATTGCRTAGTTWGGRTAGTT). To optimise the real-time PCR reaction system,
204 some DNA extracts were diluted 100-fold or 10-fold and used as a template. As
205 standards, serial plasmid dilutions of the respective functional genes (2.3×10^3 to $2.3 \times$
206 10^8 per action, $r^2 = 0.99$) were used. The 20 μL reaction mixtures included 1 μL of
207 template DNA, 12.0 μL of SYBR Premix Ex Taq (Takara BioInc, Shiga, Japan), and

https://doi.org/10.5194/bg-2020-330
Preprint. Discussion started: 8 October 2020

500 nM of each primer. All PCR runs began with an initial denaturation at 95 ℃ for 5 min, 94 °C for 1 min, 55 °C for 1 min, and 72 ℃ for 30 s. This was followed by a melting curve analysis from 65 ℃ to 98 ℃ at 0.2 ℃ per reading with a 6 s hold time. Fluorescence was read during each cycle at 83 ℃.

3. Results

3.1. Carbon content and carbon isotopic signature

The TOC content (Fig. 1A) varied from 1.3 to 4 wt.%, with a peak of 3.5–4.0 wt.% at a depth of 10–17 cm. The TOC content decreased with two steps above and below the peak. The TOC content in the 3–8 cm layer was similar to that in the 19–22 cm layer (2.2–2.3 wt.%). The TOC content in the first 2 cm and 23–24 cm layer was 1.9 and 2.2 wt.%, respectively, and was relatively constant down the core at ~1.5 wt.%.

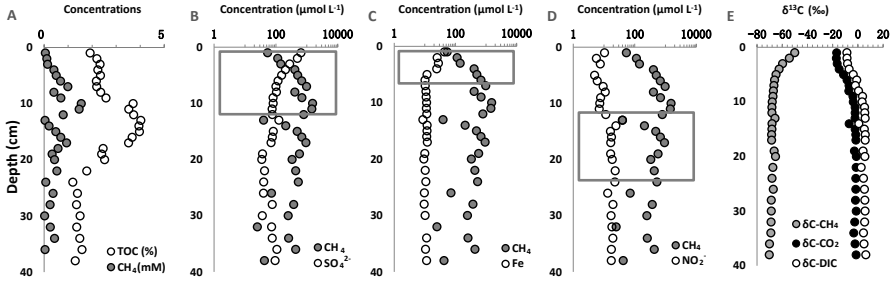

Figure. 1 *Profiles of the TOC (wt.%), methane, sulfate, iron, and nitrite in porewater. The squares in B, C, and D outline the inferred AOM zones discussed in the zonation of AOM.*

The concentration profiles of methane, nitrate, iron, and sulfate are shown in Fig. 1 (A–D). The methane concentration increased from the top surface (0.054 mM) to the 10–11 cm layer (1.5 mM), and then sharply decreased to 0.040 mM at a depth of 13 cm, it subsequently increased to 0.94 mM at a depth of 17 cm, and fluctuated between 0.025 mM and 0.58 mM below 18 cm (Fig. 1A). The sulfate concentration decrease from 0.6

https://doi.org/10.5194/bg-2020-330
Preprint. Discussion started: 8 October 2020

mM at the surface to less than 0.1 mM at a depth of 10–12 cm, which was followed by a high value at ~13 cm and then relatively constant values of 0.04–0.1 mM down the remaining core (Fig. 1B). The iron concentration declined from 44 μM at the surface to 24 μM at a depth of 4 cm, and was then relatively constant at ~10 μM down the rest of the core (Fig. 1C). The nitrite concentration decreased from 10 μM at the surface to 5 μM at a depth of 5 cm, and then increased to 40 μM at a depth of 14 cm. It subsequently reduced to 16–23 μM at a depth of 16–24 cm before remaining relatively constant down the remaining core (Fig. 1D).

The stable carbon isotopic compositions of methane, carbon dioxide, and DIC are shown in Fig. 1E. The $\delta^{13}C_{CH4}$ value (Vienna Pee Dee Belemnite, VPDB) decreased from -50.0‰ at the sediment surface to less than -68.1‰ at a depth of 11 cm, and then changed little from -68.1‰ to -70.2‰ below 12 cm (Fig. 1E). The values of $\delta^{13}C_{CO2}$ (VPDB) and $\delta^{13}C_{DIC}$ (VPDB) varied proportionally and inversely to the $\delta^{13}C_{CH4}$ values. The $\delta^{13}C_{CO2}$ and $\delta^{13}C_{DIC}$ values were almost constant for the first 3 cm (-16‰ and -8‰, respectively), and then increased below a depth of 12 cm to relatively constant values of between -1.15‰ and -2.68‰ for $\delta^{13}C_{CO2}$, and between 2.70‰ and 6.40‰ for $\delta^{13}C_{DIC}$.

3.2. Incubation results for methanogens and anaerobic methanotrophs

The incubation results for the methane production potential both with and without methanogenic substrate (i.e. acetate), and the consumption potential are shown in Fig. 2 (A–C).

https://doi.org/10.5194/bg-2020-330
Preprint. Discussion started: 8 October 2020

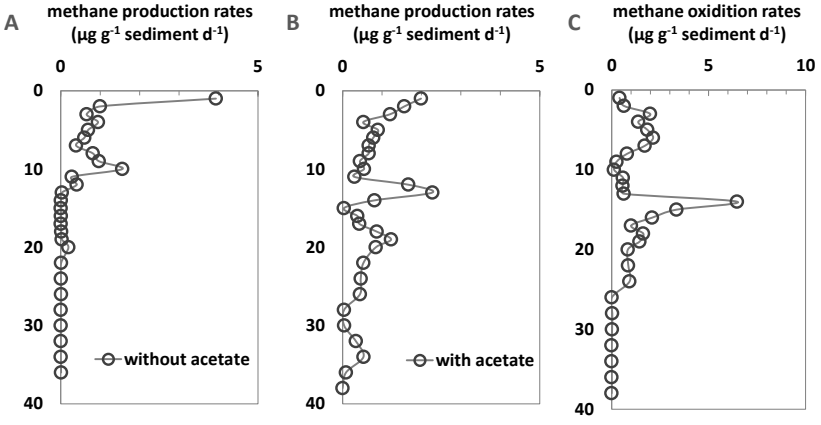

Figure. 2 *Methane production rates along the incubated sediment depth profile for cores taken from Hongfeng Reservoir: (A) without substrate, and (B) with acetate. (C) The AOM rate along the sediment depth profile for core taken from Hongfeng Reservoir.*

The methane production rate was comparatively high (0.03–3.94 μg CH_4 g^{-1} sediment d^{-1}) in sediments at a depth of 0–13 cm, and decreased down the core with the exception of that at ~20 cm (0.19 μg CH_4 g^{-1} sediment d^{-1}) (Fig. 2A). The methane production rate increased dramatically in the treatment that included acetate, especially at a depth of > 10 cm (Fig. 2B).

All of the sediments exhibited a potential of AOM within 2 months of incubation (Fig. 2C). An extremely high value (6.47 μg CH_4 g^{-1} sediment d^{-1}) was measured at a depth of ~18 cm, after which the value decreased sharply. Another active AOM zone was observed at a depth of 5–10 cm (1.37–2.14 μg CH_4 g^{-1} sediment d^{-1}).

3.3. Potential methanogen species and functional species involved in AOM

Functional molecular genetic markers that are specific to methanogens were quantified by real-time qPCR (Fig. 3A). The *mcr*A gene copy numbers were relatively constant throughout the core, although there were peaks at 12 (6.72×10^7 copies g^{-1} sediment) and 22 cm (4.92×10^7 copies g^{-1} sediment).

https://doi.org/10.5194/bg-2020-330
Preprint. Discussion started: 8 October 2020

Biogeosciences Discussions
Open Access
EGU

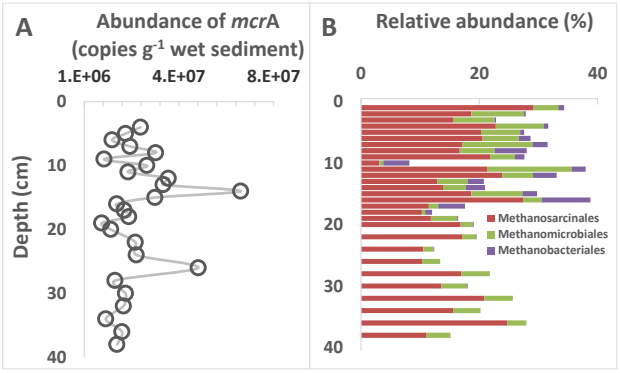

Figure. 3 *(A) Abundance of the mcrA gene, and (B) the relative abundance of dominate methanogens at the order level, as detected along the sediment depth profile in core taken from Hongfeng Reservoir.*

The archaea community in the sediments was dominated by Euryarchaeota and Bathyarchaeota, which collectively accounted for 76.0–85.1% of the total community. The main methanogens in the sediments were *Methanosarcinales* (3.09–29.18%), *Methanomicrobiales* (0.55–14.23%), and *Methanobacteriales* (0.69–8.23%) at the order level (Figs. 3B and S2). Interestingly, *Methanobacteriales* was mainly distributed at a depth of 6–18 cm (1.17–8.23%), whereas its relative abundance in the surface layer (1–5 cm) was < 0.78% and disappeared below 18 cm (< 0.01%). The abundance of *Methanomicrobiales* in the sediments was slightly higher above a depth of 15 cm (3.86–14.23%) than of that below 16 cm (0.55–4.79%).

The Illumina sequencing results showed that *Desulfobulbus* (0.10–1.96%) was present in the upper layers (0–22 cm), and that the relative abundance was higher above a depth of 9 cm (> 1%) (Fig. 4A). Some of the microorganisms that are involved in iron redox were investigated synchronously in this study, and were typical the *Ferritrophicum* and *Crenothrix* iron-oxidising bacteria (Fig. 4B) as well as the *Geobacter, Geothermobacter, Bacillus* and *Anaeromyxobacter* iron-reducing bacteria (Fig. 4C). The abundance of

https://doi.org/10.5194/bg-2020-330
Preprint. Discussion started: 8 October 2020

iron-oxidising bacteria (*Ferritrophium* and *Crenothrix*) in the sediments was higher above a depth of 17 cm (0.640–2.23%) in comparison to below 18 cm (0.23%; Fig. 4B). The total relative abundance of the four iron-reducing bacteria increased with depth, and was the highest at a depth of 19–30 cm (0.012–0.015%) (Fig. 4C). The abundance of *Anaeromyxobacter* was obviously higher throughout the sediment core in comparison to the other three iron-reducing bacteria. *Geobacter* was more abundant at a depth of < 19 cm than at shallower depths. The relative abundance of NC10 varied in a narrow range of 1.91–6.09%, with the exception of a low value of 0.83% at 14 cm (Fig. 4D). The relative abundance of nitrate reductase gradually increased from 0.041‰ to 0.076‰ above 10 cm, and subsequently fluctuated between 0.050‰ and 0.079‰ below 10 cm (Fig. 4D).

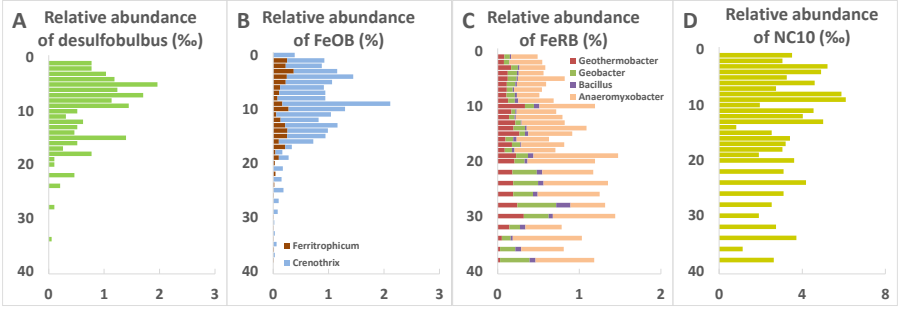

Figure. 4 *(A) Relative abundances of Desulfobulbus, (B) iron-oxidising bacteria, (C) iron-reducing bacteria, and (D) NC10 along the sediment depth profile in core taken from Hongfeng Reservoir.*

4. Discussion

4.1. Intersecting of methane production and consumption

4.1.1. Geochemical signatures

The opposite trends of the porewater profiles of the $\delta^{13}C_{CH4}$ value versus the $\delta^{13}C_{CO2}$

https://doi.org/10.5194/bg-2020-330
Preprint. Discussion started: 8 October 2020

and $\delta^{13}C_{DIC}$ (Fig. 1E) illustrate a typical zonation of methane cycle that an obvious zone of methane oxidation dominated the upper sediments (< 10 cm), and that methane production prevailed in the lower sediments (> 10 cm). When plotted against the logarithmic methane concentrations (Fig. 5), and by excluding the residual heavy methane, a linear trend of the $\delta^{13}C_{CH4}$ value suggests that methane was oxidised in the sediments, whereby the corresponding $\delta^{13}C_{DIC}$ were more positive (-8.6 ‰ to > 3 ‰ VPDB). The aerobic consumption of methane obviously occurred in the very top surface (< 1 cm) (Fig. S1) because oxygen can penetrate (< 8 mm) to this depth, even in an oligotrophic lake (Melton et al. 2014). The sediments became anaerobic while oxygen decreased rapidly with increasing sediment depth, where methane was anaerobically oxidised. The symmetrical concentration profiles of methane versus sulfate, iron, and nitrate/nitrite (Fig. 1B–D) suggest that methane oxidation may have been coupled with sulfate (< 10 cm), iron (< 5 cm) and nitrite separately (12–24 cm).

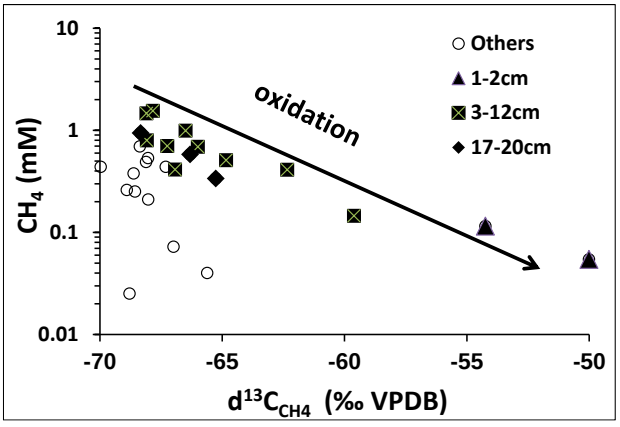

Figure. 5 *Concentration vs. carbon isotopic fractionation of methane*

4.1.2. Incubation evidence

In contrast with the geochemical signal results, the lab incubation data demonstrated

https://doi.org/10.5194/bg-2020-330
Preprint. Discussion started: 8 October 2020

the high potential of both anaerobic methane production and oxidation along the entire depth of the sediment core. Interestingly, the methane production rate was higher at a depth of 0–13 cm than that at ≥ 14 cm (Fig. 2A), and only when the extra substrate was added did the production rates increase dramatically (> 10 cm) to be higher than that in the surface sediment (Fig. 2B). In accordance with the geochemical data, an extremely high activity of methane oxidation was present at ~18 cm (Fig. 2C). Another active AOM zone was observed at 5–10 cm, which agrees with the changes in the electron acceptors (Fig. 1B, C, D). Therefore, methane production and consumption multiplied along the sediment core, and the consumption potential was much higher than production with or without extra substrate.

The coexisting methane production and oxidation was demonstrated by the two distinct production zones that were parallel to two obvious AOM zones (Fig. 2), rather than the stereotype pattern of oxidation/production along the redox gradient.

4.2. Zonation of methane production and limitation

4.2.1. Abundant methanogens along the sediments core

Abundance functional genes of methanogenic (methyl-coenzyme M reductase, *mcr*A gene) existed along the sediment core profile (Fig. 3A). This high abundance of the *mcr*A gene corresponded to the high potential of methane production within the top 10 cm.

The copy numbers of the *mcr*A gene (Fig. 3A) matched the methane production potential after substrate addition (Fig. 2B), which indicates that methanogens became active with sufficient substrate. This pattern was obvious at a depth of 10–17 cm, where

https://doi.org/10.5194/bg-2020-330
Preprint. Discussion started: 8 October 2020

the high TOC content and the anaerobic environment facilitated anaerobic digestion. The metabolic production may have also furthered promoted the growth of methanogens (e.g. via a hydrogenotrophic pathway). Therefore, the activity of methanogenesis was limited by the bioavailable substrate rather than by the abundance of methanogens.

4.2.2. Niche partitioning of various nutrient types of methanogens along the sediment core

The vertical distribution of various nutrient types of methanogens was revealed along the sediment core profile (Fig. 3B). Correspondingly, *Methanomicrobiales* and *Methanobacteriales* were mainly distributed within the upper ~20 cm. These hydrogenotrophic methanogens are able to produce methane using compounds containing H_2, CO_2, formic acid, alcohol, and propanol as energy and carbon sources. Therefore, hydrogenotrophic might have been an active methanogenic pathway in the upper layers. The relative abundance of *Methanobacteriales* peaked at 10–17 cm, and then disappeared below 18 cm (< 0.01%), which demonstrates the critical role of *Methanobacteriales* in such a fermentation layer.

The dominant methanogens were *Methanosarcinales*, which mainly consist of *Methanothrix* at the genus level, and are typical aceticlastic methanogens. When incubated with additional acetate, *Methanothrix* recovered the activity of methane production in the deeper layers. *Methanothrix* is an obligate aceticlastic methanogenic archaeon that can adapt to low concentrations of acetic acid of 7–70 μmol L^{-1} (Westermann, Ahring, and Mah 1989) due to acetyl-CoA synthetase with a high

https://doi.org/10.5194/bg-2020-330
Preprint. Discussion started: 8 October 2020

affinity to acetic acid (Jetten, Stams, and Zehnder 1990).

The functional activity, abundance, and diversity of methanogens showed a niche partitioning of various nutrient types of methanogens, mixed nutritional methanogens in the upper layer, and only aceticlastic methanogens in deeper layers. The methanogenic pathway would have changed with sediment depth, and would have been controlled by the availability of easily degradable organic matter (Deng et al. 2017) (Liu et al. 2017). In general, there is a large amount of nutrients and organic matter sequestrated in the sediments of reservoirs (e.g. acetate acid; Fig. S3). Hence, aceticlastic methanogens dominate and play a critical role in methane production in deep sediments (Scholten and Stams 2000).

4.3.Zonation of methane oxidation and metabolism

A complex oxidation pattern was revealed in the studied sediment core (Fig. 6). With the exception of the top surface layer (< 1 cm) that may have been oxidised by oxygen, methane consumption in the deeper layers was coupled with SO_4^{2-}-AOM, metal-AOM, and nitrite-AOM (Figs. 1 and 6). Mayr et al. (Mayr et al. 2020) recently found such a niche partitioning of the taxa of different methane oxidisers in four lake sediments that effectively mediated methane oxidation along with the oxygen–methane counter gradient. The functional groups involved in these processes include the consortia of anaerobic methanotrophic archaea, specific sulfate reducing bacteria (*Desulfobulbus*) (Bhattarai, Cassarini, and Lens 2019), and NC10 (Lee et al. 2018).

https://doi.org/10.5194/bg-2020-330
Preprint. Discussion started: 8 October 2020

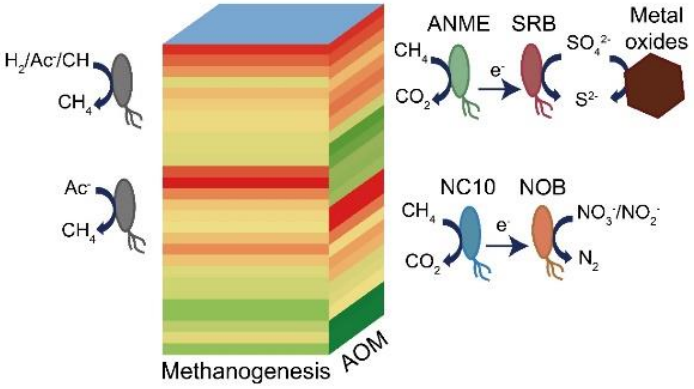

Fig. 6 *Schematic representation of methane production and oxidation along the sediment core profile. The colour represents the relative microbial activity, where red is the highest and green is the lowest. The functional groups involved in the anaerobic oxidation of methane included anaerobic methane oxidising bacteria (ANME), sulfate reducing bacteria (SRB), NC10, and nitrite oxidising bacteria (NOB).*

4.3.1. SO_4^2–AOM and metal–AOM in the subsurface layer

The profiles of oxidants and functional groups indicate that sulfate was the main oxidant for AOM in the surface layer (< 10 cm) and at ~13 cm, and subsequently drove the apparent iron oxides to mediate AOM (< 5 cm), which is similar to the report of He et al. (He et al. 2018). The relative abundance of *Desulfobulbus* in the surface layer (< 9 cm) and in the middle layer confirmed the interdependence of sulfate reducing bacteria and AOM. The reduced sulfur may have then transferred electrons to iron oxides, which could have been further driven by microbial iron oxidation performed by the identified iron-oxidising bacteria of *Ferritrophicum* and *Crenothrix* (0–17 cm). Melton et al. (Melton et al. 2014) demonstrated that Fe(II) oxidisers could overcome the competition pressure to survive in lake sediments, which resulted in a high abundance of poorly crystalline iron. Nordi et al. (Nordi, Thamdrup, and Schubert 2013) observed AOM in iron-rich freshwater lake sediments where sulfate and Fe(III) coexisted. Unfortunately,

https://doi.org/10.5194/bg-2020-330
Preprint. Discussion started: 8 October 2020

the responsible microorganisms for metal-AOM are still difficult to define, and the potential of iron-AOM is uncertain in our study due to the preferential sulfate reduction and undetected iron minerals.

4.3.2. Nitrite–AOM in the middle layer

The AOM zone in the middle layer of the sediments (14–24 cm) was confirmed by the incubation activity (Fig. 2C) and carbon isotope composition (Fig. 1E). The chemical concentrations revealed that nitrite could have been the main electron acceptor (Fig. 1D). Thomas et al. (Thomas, Perga, and Frossard 2017) found a transitional zone that hosted methanotrophic organisms (*Can. Methanoperedens*) and were able to oxidise methane by coupling nitrate reduction. Correspondingly, a typical methane anaerobic-oxidation microorganism (NC10) for nitrite dependent AOM (N-DAMO) and a relatively high abundance of nitrate reductase (> 10 cm) were also determined in the present study (Fig. 4D).

The premise of the N-DAMO reaction is the coexistence of CH_4, NO_2^-/NO_3^-, and a strictly anoxic environment (Lee et al. 2018). A high methane concentration was found at a depth of 14–24 cm (Fig. 1D) under a strictly anaerobic condition. Furthermore, biological processes such as aerobic nitrification in the microaerobic area and denitrification in the anaerobic area can produce NO_2^- (Melton et al. 2014). Therefore, the anaerobic zone of freshwater sediments is an ideal habitat for the N-DAMO reaction as reported in lake ecosystems (Deutzmann and Schink 2011), (Mayr et al. 2020).

Even a metabolic stratification has even been found in brackish coastal sediments (Egger et al. 2015), terrestrial volcanic mud (Cheng et al. 2012), and freshwater lakes

https://doi.org/10.5194/bg-2020-330
Preprint. Discussion started: 8 October 2020

(Nordi, Thamdrup, and Schubert 2013; Shen et al. 2014) . This type of complex system in sediment cores has, however, rarely been reported. The crossing pattern of methane production and consumption contributed to the geochemical patterns and microbial circumstances determined in the present study.

5. Conclusion

A complex intersecting zonation of methane production and oxidation has been revealed in the freshwater sediments based on the porewater concentration of methane, carbon isotopic composition, the incubation activity and the abundance of functional genes. Two distinct AOM zones were concurrent with two production zones. The availability of substrate, abundance and diversity of methanogens determine the production ability, the abundance and activity of functional microorganisms of AOM are crucial for quantifying the aquatic methane efflux from such environments.

The *in-situ* methane flux from the sediment to the water column was near zero during the winter, with a bottom concentration that was below the detection limit due to several filters of *in-situ* oxidation in this region. The integrated consumption capability was much higher than the production capability for the 2 month anaerobic incubation (Fig. 2). The combination of the AOM zones created multiple barriers that prevented the emission of methane to the water and atmosphere. The environmental potential of the methane emission from such reservoir sediments is less critical under current conditions. Reservoir sediments are extremely complex, and various factors such as organic carbon and different electron acceptors can affect methane production and oxidation; thus, these factors need to be comprehensively studied in different types of reservoirs. This

https://doi.org/10.5194/bg-2020-330
Preprint. Discussion started: 8 October 2020

study sheds new light on the metabolism and mechanism behind the methane production and oxidation in reservoir sediments, which can help to better remedy the widespread methane emissions from freshwater sediments.

Author contribution: F. Wang conceived and supervised the study. L. Liu, X. Chen designed the experiments. X. Chen, J. Yu, F. Bai, M. Yang, S. Bai and Z. Chen performed the experiments. X. Chen, F. Bai, S. Bai, C. He and X. Liu analyzed the data. .X. Chen, L. Liu, Z. Chen, J. Yu and J. Sun wrote the manuscript.

Competing interests: The authors declare that they have no conflict of interest.

Acknowledgements

This work was supported by the National Key Research and Development Project by Most of China (grant number 2016YFA0601000), National Natural Science Foundation of China (grant numbers 41776071, 41073072, 21677093), the Shanghai Science and Technology Committee (grant number 12231202004), Guangdong MEPP Fund (NO. GDOE[2019]A41).

Reference

Barros, N., Cole, J.J., Tranvik, L.J., Prairie, Y.T., Vera D.B., Huszar, L.M., Giorgio del P., and Roland, F., 2011. Carbon emission from hydroelectric reservoirs linked to reservoir age and latitude. Nature Geosci. 4, 593-596.

Bastviken, D., Cole, J.J., Pace, M., Tranvik. L., 2004. Methane emissions from lakes: Dependence of lake characteristics, two regional assessments, and a global estimate. Global Biogeochem. Cy. 18, GB4009.

Bastviken, D., Cole, J.J., Pace, M.L., Van de Bogert, M.C., 2008. Fates of methane from different lake habitats: Connecting whole-lake budgets and CH_4 emissions. J. Geophys. Res.-Biogeosci. 113, G02024.

Beal, E.J., House, C.H., Orphan, V.J., 2009. Manganese- and iron-dependent marine methane oxidation. Science 325, 184-187.

Bhattarai, S., Cassarini, C., Lens, P. N. L., 2019. Physiology and distribution of archaeal methanotrophs that couple anaerobic oxidation of methane with sulfate reduction. Microbiol. Molec. Biol. Rev. 83, e00074-18.

Caporaso, J.G., Lauber, C.L., Walters, W.A., Berg-Lyons, D., Huntley, J., Fierer, N., Owens, S.M., Betley, J., Fraser, L., Bauer, M., Gormley, N., Gilbert, J.A., Smith, G. Knight. R., 2012. Ultra-high-

https://doi.org/10.5194/bg-2020-330
Preprint. Discussion started: 8 October 2020

throughput microbial community analysis on the Illumina HiSeq and MiSeq platforms. ISME J. 6, 1621-1624.

Cheng, T.W., Chang, Y.H., Tang, S.L., Tseng, C.H., Chiang, P.W., Chang, K.T., Sun, C.H., Chen, Y.G., Kuo, H.C., Wang, C.H., Chu, P.H., Song, S.R., Wang, P.L., Lin. L.H., 2012. Metabolic stratification driven by surface and subsurface interactions in a terrestrial mud volcano. ISME J. 6, 2280-2290.

Crowe, S.A., Katsev, S., Leslie, K., Sturm, A., Magen, C., Nomosatryo, S., Pack, M.A., Kessler, J.D., Reeburgh, W.S., Roberts, J.A., Gonzalez, L., Haffner, G.D., Mucci, A., Sundby, B., Fowle, D. A., 2011. The methane cycle in ferruginous Lake Matano. Geobiology 9, 61-78.

Deemer, B.R., Harrison, J.A., Li, S., Beaulieu, J.J., Delsontro, T., Barros, N., Bezerra-Neto, J.F., Powers, S.M., dos Santos, M.A., Vonk, J.A., 2016. Greenhouse gas emissions from reservoir water surfaces: a new global synthesis. Bioscience 66, 949-964.

Deng, Y., Liu, Y., Dumont, M., Conrad, R., 2017. Salinity affects the composition of the aerobic methanotroph community in alkaline lake sediments from the Tibetan Plateau. Microbial. Ecol. 73,101-110.

Deutzmann, J.S., Schink, B., 2011. Anaerobic oxidation of methane in sediments of Lake Constance, an oligotrophic freshwater lake. Appl. Environ. Microbiol. 77, 4429-4436.

Egger, M., Rasigraf, O., Sapart, C.J., Jilbert, T., Jetten, M.S.M., Rockmann, T., van der Veen, C., Banda, N., Kartal, B., Ettwig, K.F., Slomp, C.P., 2015. 'Iron-mediated anaerobic oxidation of methane in brackish coastal sediments. Environ. Sci. Technol. 49, 277-283.

Ettwig, K.F., Butler, M.K., Le Paslier, D., Pelletier, E., Mangenot, S., Kuypers, M.M., M. Schreiber, F., Dutilh, B. E., Zedelius, J., de Beer, D., Gloerich, J., Wessels, H. J.C.T., van Alen, T., Luesken, F., Wu, M.L., van de Pas-Schoonen, K.T., Op den Camp, H.J.M., Janssen-Megens, E.M., Francoijs, K., Stunnenberg, H., Weissenbach, J., Jetten, M.S.M., Strous, M., 2010. Nitrite-driven anaerobic methane oxidation by oxygenic bacteria. Nature 464, 543-548.

Evans, P.N., Boyd, J.A., Leu, A.O., Woodcroft, B.J., Parks, D.H., Hugenholtz, P., Tyson G.W., 2019. An evolving view of methane metabolism in the Archaea, Nat. Rev. Microbiol. 17, 219-232.

Goldman, A.E., Cadieux, S.B., White, J.R., Pratt, L.M., 2016. Passive sampling method for high-resolution concentration and isotopic composition of dissolved methane in Arctic lakes. Limnol. Oceanogr.-Meth. 14, 69-78.

He, Z., Wang, J., Hu, H,. Yu, M., Jetten, S. M. Liu, H., Cai, C., Liu, Y., Ren, H., Zhang, X., Hua, M., Xu, X., Zheng, P., Hu. B., 2019. Regulation of coastal methane sinks by a structured gradient of microbial methane oxidizers. Environ. Pollu. 244, 228-237.

He, Z., Zhang, Q., Feng, Y., Luo, H., Pan, X., Gadd. G.M., 2018. Microbiological and environmental significance of metal-dependent anaerobic oxidation of methane. Sci. Total Environ. 610, 759-768.

Jetten, M.S.M., Stams, A.J.M., Zehnder, A.J.B., 1990. Acetate threshold values and acetate activating enzymes in methanogenic bacteria. FEMS Microbiol. Ecol. 73, 339-344.

Lee, H.S., Tang, Y., Rittmann, B.E., Zhao, H.P., 2018. Anaerobic oxidation of methane coupled to denitrification: fundamentals, challenges, and potential. Critical Reviews in Environ. Sci. Technol. 48,1067-1093.

Liu, Y., Conrad, R., Yao, T., Gleixner, G., Claus, P., 2017. Change of methane production pathway with sediment depth in a lake on the Tibetan plateau. Palaeogeogr. Palaeoclimatol. Palaeoecol. 474, 279-286.

https://doi.org/10.5194/bg-2020-330
Preprint. Discussion started: 8 October 2020

522 Maeck, A., DelSontro, T., McGinnis, D.F., Fischer, H., Flury, S., Schmidt, M., Fietzek, P., Lorke, A.,
523 2013. Sediment trapping by dams creates methane emission hot spots. Environ. Sci. Technol.
524 47, 8130-8137.
525 Maltby, J., Steinle, L., Loescher, C.R., Bange, H.W., Fischer, M.A., Schmidt, M., Treude, T., 2018.
526 Microbial methanogenesis in the sulfate-reducing zone of sediments in the Eckernforde Bay,
527 SW Baltic Sea. Biogeosciences 15, 137-157.
528 Mayr, M.J., Zimmermann, M., Guggenheim, C., Brand, A., Buergmann, H., 2020. Niche partitioning of
529 methane-oxidizing bacteria along the oxygen-methane counter gradient of stratified lakes.
530 ISME J. 14, 274-287.
531 Melton, E., Stief, P., Behrens, S., Kappler, A., Schmidt, C., 2014. High spatial resolution of distribution
532 and interconnections between Fe- and N-redox processes in profundal lake sediments. Environ.
533 Microbiol. 16, 3287-3303.
534 Mendonça, R., Barros, N., Vidal, L.O., Pacheco, F., Kosten, S., Roland, F., 2012. Greenhouse gas
535 emissions from hydroelectric reservoirs: what knowledge do we have and what is lacking? in
536 Liu G. X., (ed.), Greenhouse gases-emission, measurement and management (Springer).
537 Nordi, K.A., Thamdrup. B., 2014. Nitrate-dependent anaerobic methane oxidation in a freshwater
538 sediment. Geochim. Cosmochim. Acta 132, 141-150.
539 Nordi, K.A., Thamdrup, B., Schubert C.J., 2013. Anaerobic oxidation of methane in an iron-rich Danish
540 freshwater lake sediment. Limnol. Oceanogr. 58, 546-554.
541 Riedinger, N., Formolo, M.J., Lyons, T.W., Henkel, S., Beck, A., Kasten, S., 2014. An inorganic
542 geochemical argument for coupled anaerobic oxidation of methane and iron reduction in marine
543 sediments. Geobiology 12, 172-181.
544 Scholten, J.C.M., Stams, A.J.M., 2000. Isolation and characterization of acetate-utilizing anaerobes from
545 a freshwater sediment. Microb. Ecol. 40, 292-299.
546 Schonheit, P., Kristjansson J.K., Thauer R.K., 1982.'kinetic mechanism for the ability of sulfate reducers
547 to out-compete methanogens for acetate. Arch. Microbiol. 132, 285-288.
548 Shen, L., Liu, S., Zhu, Q., Li, X., Cai, C., Cheng, D., Lou, L., Xu, X., Zheng, P., Hu, B., 2014. Distribution
549 and diversity of nitrite-dependent anaerobic methane-oxidising bacteria in the sediments of the
550 Qiantang River. Microb. Ecol. 67, 341-349.
551 Sivan, O., Adler, M., Pearson, A., Gelman, F., Bar-Or, I., John, S.G., Eckert, W., 2011. Geochemical
552 evidence for iron-mediated anaerobic oxidation of methane. Limnol. Oceanogr. 56, 1536-1544.
553 Szafranek-Nakonieczna, A., Pytlak, A., Grzadziel, J., Kubaczynski, A., Banach, A., Gorski, A.,
554 Goraj, W., Kuzniar, A., Galazka A., Stepniewska, Z., 2019. Changes in the substrate source
555 reveal novel interactions in the sediment-derived methanogenic microbial community. Int. J.
556 Mol. Sci. 20(18), 4415
557 Thomas, C., Perga, M.E., Frossard,V., 2017. In vertical structure and horizontal variations in the cycling
558 of methane in the sediment of Lake Onego, Russia. In EGU. General Assembly Conference.
559 Vienna.
560 Wassmann, R., Neue, H.U., Bueno, C., Lantin, R.S., Alberto, M.C.R., Buendia, L.V., Bronson, K., Papen,
561 H., Rennenberg H., 1998. Methane production capacities of different rice soils derived from
562 inherent and exogenous substrates. Plant Soil 203, 227-237.
563 Westermann, P., Ahring, B.K., Mah, R.A. 1989. Threshold acetate concentrations for acetate catabolism
564 by aceticlastic methanogenic bacteria. Appl. Environ. Microbiol. 55, 514-515.